Do Assimilated Drifter Velocities Improve Lagrangian Predictability in an Operational Ocean Model?

PHILIP MUSCARELLA, MATTHEW J. CARRIER, HANS NGODOCK, AND SCOTT SMITH

Naval Research Laboratory, Stennis Space Center, Mississippi

B. L. LIPPHARDT JR., A. D. KIRWAN JR., AND HELGA S. HUNTLEY

School of Marine Science and Policy, University of Delaware, Newark, Delaware

(Manuscript received 28 May 2014, in final form 8 December 2014)

ABSTRACT

The Lagrangian predictability of general circulation models is limited by the need for high-resolution data streams to constrain small-scale dynamical features. Here velocity observations from Lagrangian drifters deployed in the Gulf of Mexico during the summer 2012 Grand Lagrangian Deployment (GLAD) experiment are assimilated into the Naval Coastal Ocean Model (NCOM) 4D variational (4DVAR) analysis system to examine their impact on Lagrangian predictability. NCOM-4DVAR is a weak-constraint assimilation system using the indirect representer method. Velocities derived from drifter trajectories, as well as satellite and in situ observations, are assimilated. Lagrangian forecast skill is assessed using separation distance and angular differences between simulated and observed trajectory positions. Results show that assimilating drifter velocities substantially improves the model forecast shape and position of a Loop Current ring. These gains in mesoscale Eulerian forecast skill also improve Lagrangian forecasts, reducing the growth rate of separation distances between observed and simulated drifters by approximately 7.3 km day^{-1} on average, when compared with forecasts that assimilate only temperature and salinity observations. Trajectory angular differences are also reduced.

1. Introduction

The importance of Lagrangian forecasts was seen in the wake of the Deepwater Horizon oil spill in the northern Gulf of Mexico (GOM). The agencies responding to this disaster required information about the transport and dispersion of water parcels and in turn oil. Unfortunately, while numerical models and data assimilation methods continue to improve, trajectory forecasts remain challenging.

A number of studies have investigated Lagrangian predictability using model velocities and observed drifter trajectories (Thompson et al. 2003; Özgökmen et al. 2003; Barron et al. 2007; Huntley et al. 2011). These studies show that model trajectory uncertainties typically grow rapidly, often on the order of 0.5–1 km h^{-1}. This is likely due to small model velocity uncertainties that accumulate during trajectory integration (Huntley et al. 2011). Model forecast velocities remain prone to errors due to the lack of observations available for assimilation and validation. Increasing model resolution aggravates this problem, since even more observations are needed to constrain the smaller scales that are resolved. As more observations become available in the future, the constraints they provide through assimilation should directly translate into improved trajectory forecast skill.

The types of observations assimilated and their spatial and temporal resolution also play an important role. Temperature, salinity, and sea surface height (SSH, measured along-track by satellite altimeters) observations are typically assimilated in operational ocean models. However, it should be noted that along-track SSH observations are not assimilated directly; they are used to calculate synthetic profiles of temperature and salinity, and it is these synthetic profiles that are assimilated. Since these observations directly constrain only the model mass field, thus influencing only the barotropic component of the flow, their impact on trajectory forecast skill is unclear. In addition, SSH measurements

Corresponding author address: Philip Muscarella, Naval Research Lab, 1009 Balch Blvd., Stennis Space Center, MS 39522-5001.
E-mail: philip.muscarella@nrlssc.navy.mil

DOI: 10.1175/MWR-D-14-00164.1

are highly resolved in space and time along the satellite track, but are coarsely resolved in the cross-track direction with track repeat intervals as long as 10 days. When assimilated, the disparity in space and time scales of the altimeter measurements lead to biases in the mesoscale forecasts that are very difficult to quantify (Jacobs et al. 2014a). These biases certainly impact the skill of model trajectory forecasts.

When adding assimilation of Lagrangian trajectories (or their derived velocities) to the typical assimilation constraints on the model mass fields, the trajectory forecast skill improves. A variety of methods have been explored for assimilating Lagrangian information into ocean models. Toner et al. (2001) used a normal mode analysis method with constrained optimization to minimize changes in model velocities while matching velocities along trajectories. Kuznetsov et al. (2003) and Ide et al. (2002) presented a method for the direct assimilation of Lagrangian data using augmented tracer advection equations that track the correlations between the flow and the tracers using an extended Kalman filter. Molcard et al. (2005) used a statistical method to correlate model and drifter velocities. Taillandier et al. (2006) describe the Lagrangian variational analysis (LAVA) method that minimizes the distance between observed and model drifter positions. Additionally, Nodet (2006) presents an identical twin experiment using four-dimensional variational data assimilation (4DVAR) in an idealized wind-driven midlatitude box model. These previous studies focused on sequential methods or variational techniques applied to simplified or idealized ocean models with simulated data.

Using synthetic data from a model control run, Vernieres et al. (2011) showed that the assimilation of trajectory data is surprisingly effective in constraining the model SSH field to capture eddy shedding events, much more so than the assimilation of comparable Eulerian velocity data. Assimilating trajectory positions carries with it the challenge of estimating appropriate covariances. This problem is circumvented if derived velocities are used instead. Carrier et al. (2014) demonstrated significant improvements in forecast skill in model velocity, salinity, and SSH fields when velocities derived from drifters were assimilated in addition to Eulerian observations. This study goes a step further and seeks to quantify how Lagrangian forecast skill is affected by the assimilation of drifter-derived velocities. For this purpose, the series of experiments conducted by Carrier et al. (2014), using a dynamically consistent 4D variational approach to assimilate velocities derived from roughly 300 observed drifters in the northern GOM into an operational ocean model, is analyzed for their skill in predicting future drifter trajectories. Additionally, a first step toward determining the spatial extent of these Lagrangian prediction improvements is undertaken with a drastic data-denial experiment.

This paper is organized as follows. In section 2 the model and assimilation system are described. In section 3 the observations and the data processing are discussed. The methods used computing model trajectories and their comparison with observations is discussed in section 4. Trajectory forecast skill results are described in section 5. Finally, section 6 provides a summary and conclusions.

2. Model and data assimilation system

The model used here is a GOM regional version of the U.S. Navy Coastal Ocean Model (NCOM), a free-surface primitive equation model that uses hybrid generalized vertical coordinates (Martin 2000). NCOM is used operationally to produce forecasts of temperature, salinity, velocity, and SSH for numerous global and regional applications.

The GOM regional NCOM domain spans 18°–31°N latitude and 79°–98°W longitude with a horizontal resolution of 6 km. Of the 50 vertical layers, the top 10 are free sigma followed by 40 z levels extending down to 5500 m. The initial and boundary conditions are taken from a global NCOM model with 1/8° resolution. Atmospheric forcing fields (wind stress, atmospheric pressure, and heat flux) are taken from the Navy Operational Global Atmospheric Prediction System (NOGAPS) with 0.5° horizontal resolution (Rosmond et al. 2002).

The assimilation system used here, NCOM-4DVAR, is dynamically consistent with the physics and numerics of NCOM. NCOM-4DVAR uses the indirect representer method developed by Egbert et al. (1994), Chua and Bennett (2001), and Bennett (2002). See Ngodock (2005) and Ngodock and Carrier (2013) for more details. The velocity and mass field corrections to the forward model are connected by a barotropic model with linearized covariance matrix operators.

Here, NCOM-4DVAR is run in a weak-constraint mode, so that possible errors in the model dynamics are included in the assimilation, in addition to initial condition errors (Ngodock and Carrier 2014). The initial errors at the surface are set to 2°C for temperature, 0.5 psu for salinity, 0.2 m s^{-1} for u and v velocity, and 0.1 m for SSH. These errors are attenuated with increasing depth (Yu et al. 2012). This specification is appropriate because maximum errors are expected at the surface due to uncertainties in atmospheric forcing. The error magnitudes represent 10% of the average surface forcing fields over the assimilation window. This choice is consistent with that of Carrier et al. (2014). The

choice of 10% is deemed acceptable as ocean surface currents are strongly influenced by surface wind stress. The horizontal attenuation length scales of both the initial and model errors range from 30 to 40 km, corresponding to the Rossby radius of deformation in the GOM. While the background error scales are static through time, the flow-dependent, time-evolving scales are applied by the dynamics from the tangent linear and adjoint models of NCOM.

Each observation is also assigned an error value. Observation errors include both estimated instrument error and representative error. Representative errors account for processes unresolved by the model. A comparison between our experiments and a higher-resolution (3 km) reanalysis (named RT3km_v2 in Jacobs et al. 2014b) shows that the variance of the difference of surface velocities is approximately 0.03 m s^{-1} and is subsumed into the larger observational error. Observation errors are assumed to be constant in time, with values of 0.2°C for temperature, 0.1 psu for salinity, and 0.05 m s^{-1} for velocity. These temperature and salinity errors are representative of values used by the operational data processing system used by the U.S. Navy. As noted by Carrier et al. (2014), the assumed velocity observation error results from drifter position uncertainties (10 m) and the time interval between positions (15 min). The velocity observation error (0.02 m s^{-1}) was conservatively estimated as the worst case, with maximum error in both drifter positions totaling 20 m.

3. Observations and data processing

During the Grand Lagrangian Deployment (GLAD), the Consortium for Advanced Research on Transport of Hydrocarbons in the Environment (CARTHE) deployed roughly 300 CODE-type surface drifters (drogued at 1 m) in the northern GOM at the end of July 2012 (Poje et al. 2014). These drifters were tracked using commercially available GPS units, and reported their positions via satellite roughly every 5 min.

For this analysis, GLAD drifter positions were assumed to be accurate to within 10 m. The GPS manufacturer specifies an accuracy of 6.4 m. A dock-side test verified that 98% of reported positions were within 10 m of the mean measurement for each of 10 drifters over a 12-h period. Initial position uncertainty of this magnitude leads to endpoint uncertainty for model trajectories after 96 h on the order of 200 m. Thus, both observed and modeled position uncertainties are negligible relative to the model errors discussed below.

A drifter position record was terminated at the point where the signal was lost for more than 24 h, if the drifter was known to be picked up by a boat, or if it traveled more than 80 km in a 12-h period (implying a mean speed of 1.85 m s^{-1} over 12 h).

Infrequent large errors were found in the GLAD drifter position records, typically due to poor GPS satellite reception. These outliers were identified and removed by a three-step procedure: 1) positions that implied instantaneous drifter speeds greater than 3 m s^{-1} were deleted, 2) positions that implied a drifter track that rotated through more than 360 compass degrees within 3 hours were deleted, and 3) each remaining position was estimated with a local spline interpolation using past and future—but not the current—positions from the same drifter. Measured positions that deviated more than 100 m from the corresponding spline estimate were deleted.

When all outliers were removed, record gaps were filled by spline interpolation of the remaining valid positions to uniform 5-min intervals. Estimates of u (east–west) and v (north–south) velocities were computed from these 5-min records using second-order, centered finite differences.

To reduce noise, the 5-min position and velocity records were filtered using a fourth-order Butterworth low-pass filter with a 1-h period cutoff. Finally, the low-pass-filtered records were subsampled at uniform 15-min intervals beginning on whole hours. The GLAD trajectory dataset used here is publicly available (https://data.gulfresearchinitiative.org/data/R1.x134.073:0004/). Figure 1 shows a time series of the number of GLAD trajectories available for each 12-h window during the study period.

Additional assimilated observations include GOES-East sea surface temperature (SST), ARGO profiling floats (Roemmich et al. 2001), and expendable bathythermographs (XBT). These represent typical observation types and distributions for the region of interest. The quality control and preparation of these observations is performed by the NCODA system (Cummings 2005). Note that the vast majority of these observations are SST data.

The time period for the analysis presented here is 1 August–30 September 2012. During this period, a large Loop Current eddy (evident in the 23 August SSH field shown in Fig. 2) was present in the mid-GOM. Figure 3 shows that the GLAD trajectories covered much of the northeastern GOM during this period, with several preferred pathways evident. Velocities derived from these drifter trajectories help to constrain the mesoscale features of the model forecasts. An important event during the study period was the passage of Hurricane Isaac, a category 1 hurricane, during 26–30 August 2012. The storm was responsible for the sharp drop in the

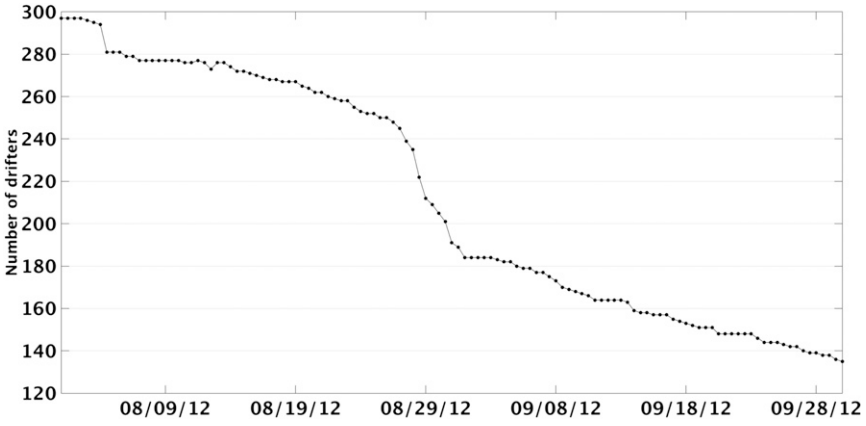

FIG. 1. Number of GLAD drifters during the study period.

number of reporting drifters seen in Fig. 1. It also spread the remaining drifters over a much larger area of the GOM. While not quantifiable, it is possible that the loss in numbers was compensated for by better spatial coverage.

4. Methods

In this section, two NCOM-4DVAR model forecast experiments with assimilation are compared with a free-running NCOM model without any assimilation. The

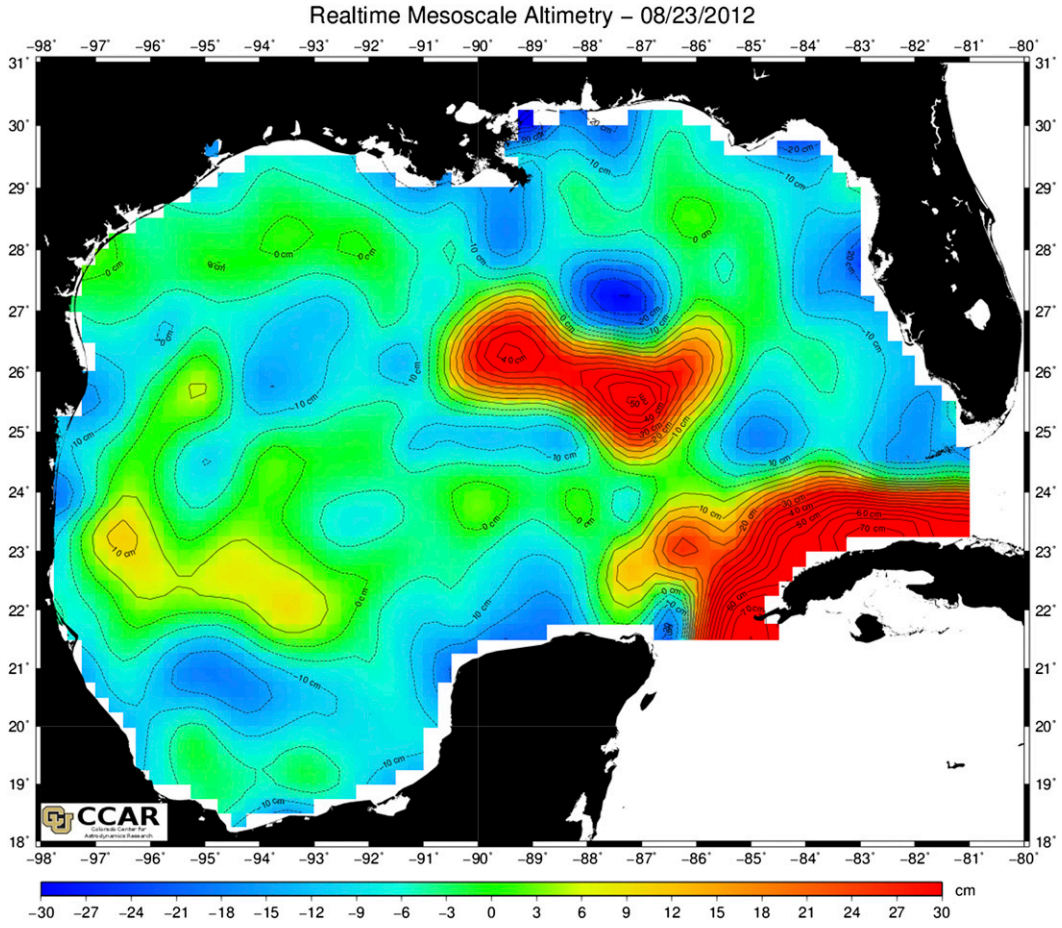

FIG. 2. Composite GOM SSH field showing the position of a Loop Current ring on 23 Aug 2012. [Courtesy of Colorado Center for Astrodynamics Research (CCAR).]

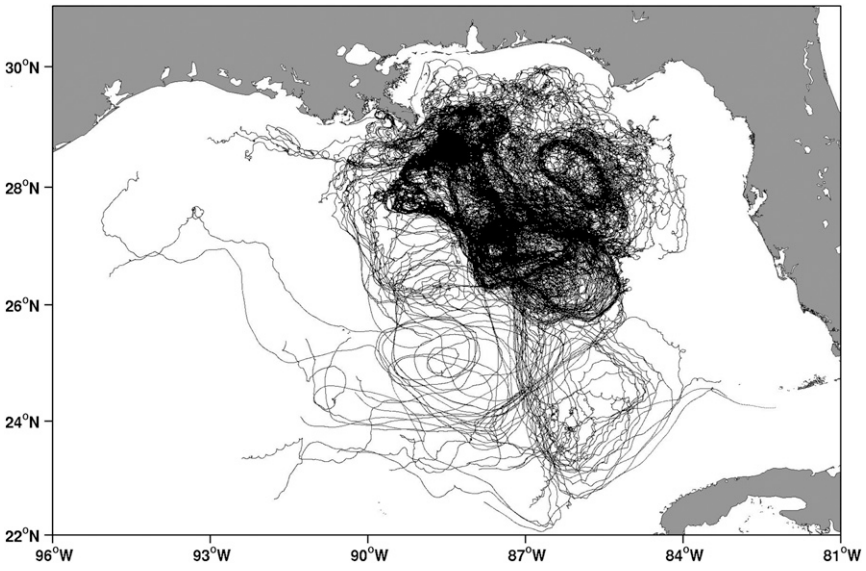

FIG. 3. GLAD drifter trajectories for the period 1 Aug–30 Sep 2012.

free running experiment is referred to as the ''FREE'' run. The first assimilative forecast uses only temperature and salinity observations and it is referred to as the ''T/S'' run. The second assimilative forecast uses temperature, salinity, and velocities from the GLAD drifters and it is referred to as the ''ALL'' run. The two assimilative forecasts were run as described in Carrier et al. (2014). Here ''assimilative forecasts'' refers to those forecasts initialized from the assimilation analysis.

The T/S and ALL forecasts use 4-day assimilation windows throughout the study period. After each 4-day assimilation cycle, 4-day forecasts are produced by the forward model using the corrected end state of the previous assimilation cycle as the initial condition. The 4-day forecasts are later used as the background for the next 4-day assimilation window. As described by Carrier et al. (2014), data injection every hour during the assimilation period produced the best fit to the observations. All data each hour was spatially subsampled to match the spatial correlation length. The relatively long forecast window of 4 days was chosen to achieve a reasonable level of independence between assimilated and evaluation data.

Simulated trajectories are computed for each NCOM forecast using simple advection. No attempt is made to account for subgrid scale or diffusion effects. Simulated drifters are advected with hourly model surface velocities (linearly interpolated in space and time) using an explicit, adaptive time-step fourth-order Runge–Kutta scheme. The initial locations of the simulated drifters are set as the locations of the GLAD drifters at the start time of each 4-day forecast.

Two metrics are used to compare GLAD trajectories with simulated trajectories from all three NCOM forecasts. The first metric is *separation distance*, computed as the distance (in kilometers) between an observed and simulated drifter at a specified time. This metric is frequently used to assess trajectory forecast skill (e.g., see Huntley et al. 2011). The second metric is *angular difference*, used to investigate possible direction biases in model forecasts. A drifter angle is defined as the compass angle of the line drawn between the drifter launch position and its position at a specified time. The *angular difference* is defined as the difference (in degrees) between observed and simulated drifter angles. These metrics are computed using all available GLAD trajectories.

5. Results

Figure 4 shows a time series of mean separation distance (computed using all available GLAD trajectories) 24 h into the 4-day forecast for all three NCOM runs over the 14 assimilation intervals in the study period. Over the entire study period, the ALL run produces the smallest separation distances, with a mean value of approximately 10 km. Separation distance for the ALL run also decreases with time as the model is repeatedly corrected with the observed velocities. Separation distances after 48, 72, and 96 h (not shown) show similar behavior over time, with larger magnitudes. It is also interesting to note that the assimilation of just temperature and salinity does not outperform the FREE run in

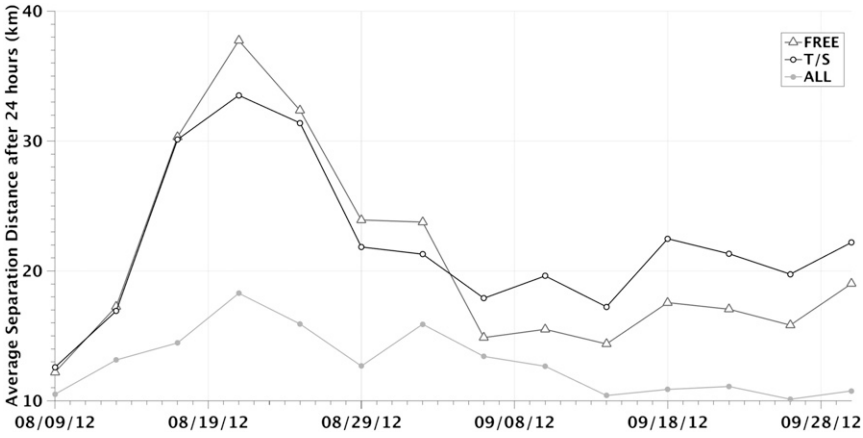

FIG. 4. Mean separation distance (km) after 24 h between the GLAD and simulated drifters for each assimilation cycle. The average is taken over all the available drifters at each time.

predicting velocity trajectories (especially toward the later part of the experiment). This decrease in forecast skill, due to the low predictability of the ocean response to hurricanes, coupled with the ageostrophic conditions that persist in the wake of a passing hurricane, make the constraining of surface velocities with temperature and salinity observations difficult.

Separation distances for the FREE run and T/S forecasts peak on 21 August, after the fourth assimilation cycle (Fig. 4). For the ALL forecast, which assimilates GLAD velocities, this peak is reduced markedly. The peak on 21 August is due to forecast errors (most noticeable in the T/S and FREE runs) in the position and shape of the Loop Current ring. Figures 5a and 5b show the mean FREE and T/S forecast SSH field computed over the period 21–25 August 2012, as well as some example GLAD and model trajectories. There is an obvious mismatch between the GLAD trajectories and the mean FREE and T/S forecast SSH. Figure 5c shows the mean ALL forecast SSH field computed over the same time period. The ALL forecast produces a better realization of the Loop Current ring yielding much better agreement between the GLAD and simulated drifters. For the ALL forecast (Fig. 5c) both the observed and simulated trajectories follow the ring boundary, consistent with geostrophic flow. The Loop Current ring shape in Fig. 5c agrees very well with the composite altimetry map for 23 August shown in Fig. 2. The assimilation of the velocity data improves the SSH field due to the dynamical connection between the mass and velocity fields provided by the barotropic model. The extent of this Eulerian improvement is explored more fully in a companion paper (Carrier et al. 2014).

Time series of separation distance, computed hourly as the average over all available drifters, for the 96-h forecast of each assimilation cycle are shown for the FREE forecasts (Fig. 6a), the T/S forecasts (Fig. 6b), and the ALL forecasts (Fig. 6c). In these figures, one curve is shown for each of the 14 assimilation cycles during the study period. The ALL forecasts (Fig. 6c) consistently produce better trajectory forecasts, with much lower separation distances over all cycles when compared to the FREE (Fig. 6a) and T/S forecasts (Fig. 6b). When the 14 curves in Figs. 6a–c are averaged, linear fits to the curve show a 12.5 km day^{-1} increase in separation distance for the ALL forecasts compared to 19.8 km for the T/S forecasts and an 18.6 km day^{-1} for the FREE forecasts. Figure 6 also shows the increased spread of the separation distance enveloped for the FREE and T/S forecasts when compared to the ALL forecasts.

Time series of the distributions of angular differences are best presented as two-dimensional histograms. Histograms of angular differences after 24-h forecasts are shown for the FREE forecasts (Fig. 7a), T/S forecasts (Fig. 7b), and the ALL forecasts (Fig. 7C). For these histograms, angular differences were binned in 15° intervals. A comparison among Figs. 7a–c shows that the ALL forecasts produce smaller angular differences, with most angular differences ranging from approximately −60° to 60°. The FREE and T/S experiments (Figs. 7a and 7b) have more drifters with larger angular differences. The histograms in Fig. 7 do not show any obvious preferred directional mismatch, with most angular differences ranging from approximately −45° to 45°.

To assess the potential spatial range of our model corrections for improving Lagrangian predictability, a data-denial experiment was performed, where approximately 50% of the original drifter record was left out for validation. Figure 8 shows the trajectories of the included drifters as well as a 50-km-radius circle. Any

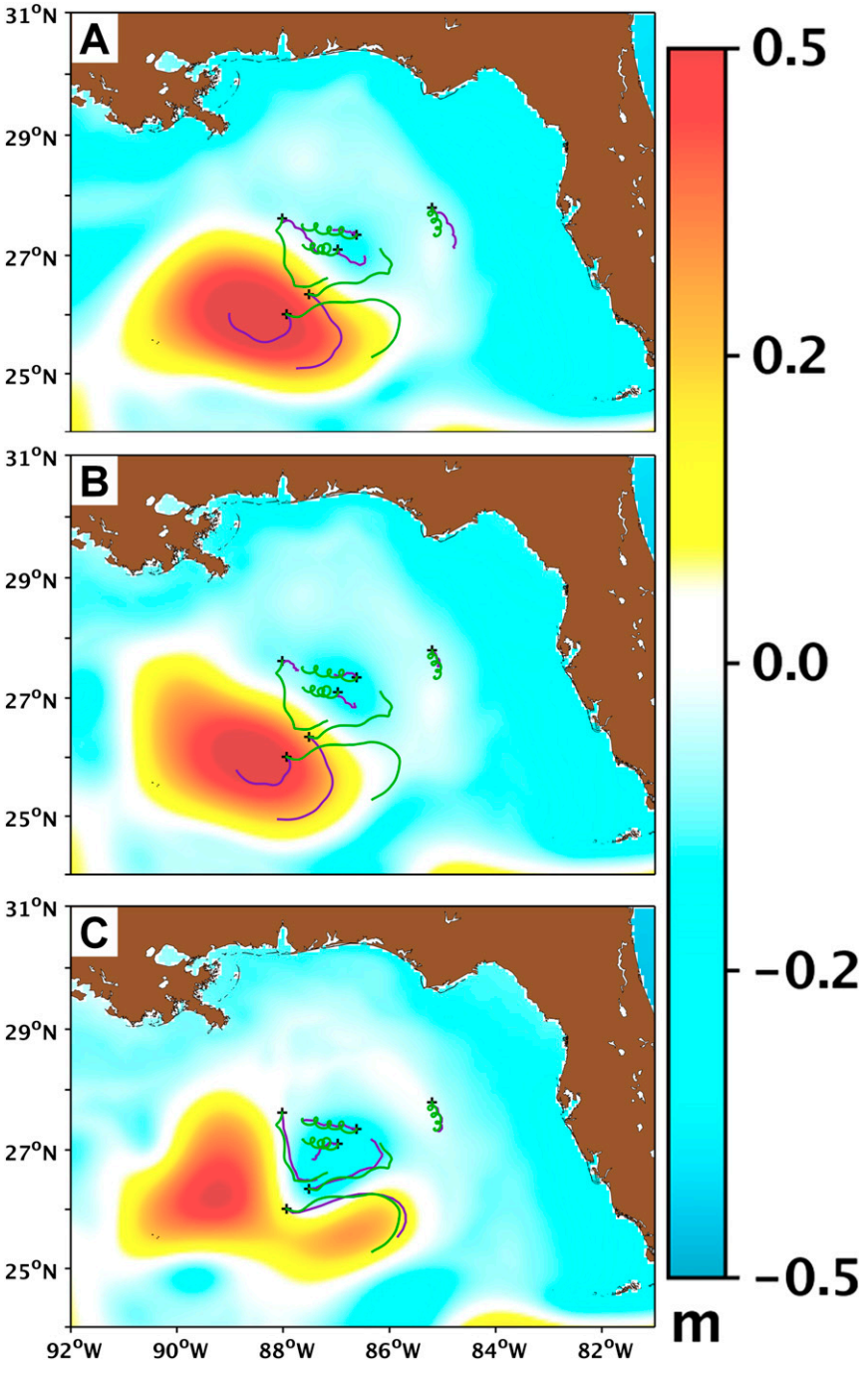

FIG. 5. Mean SSH (m) for the (a) FREE experiment, (b) T/S experiment, and (c) ALL experiment for 0000 UTC 21 Aug–0000 UTC 25 Aug 2012. Black crosses indicate observed positions at 0000 UTC 21 Aug 2012 for six GLAD drifters. Observed (green) and simulated (purple) trajectories using (a) FREE, (b) T/S, and (c) ALL forecast velocities are also shown.

drifter that entered that circle during the 2-month study period was removed from the assimilation. This location was chosen to make this test as rigorous as possible by removing a large number of drifters that observe the mesoscale eddy that is a main circulation feature in this domain.

Figure 9a shows the separation distance time series similar to Fig. 4 except that the separation distance is

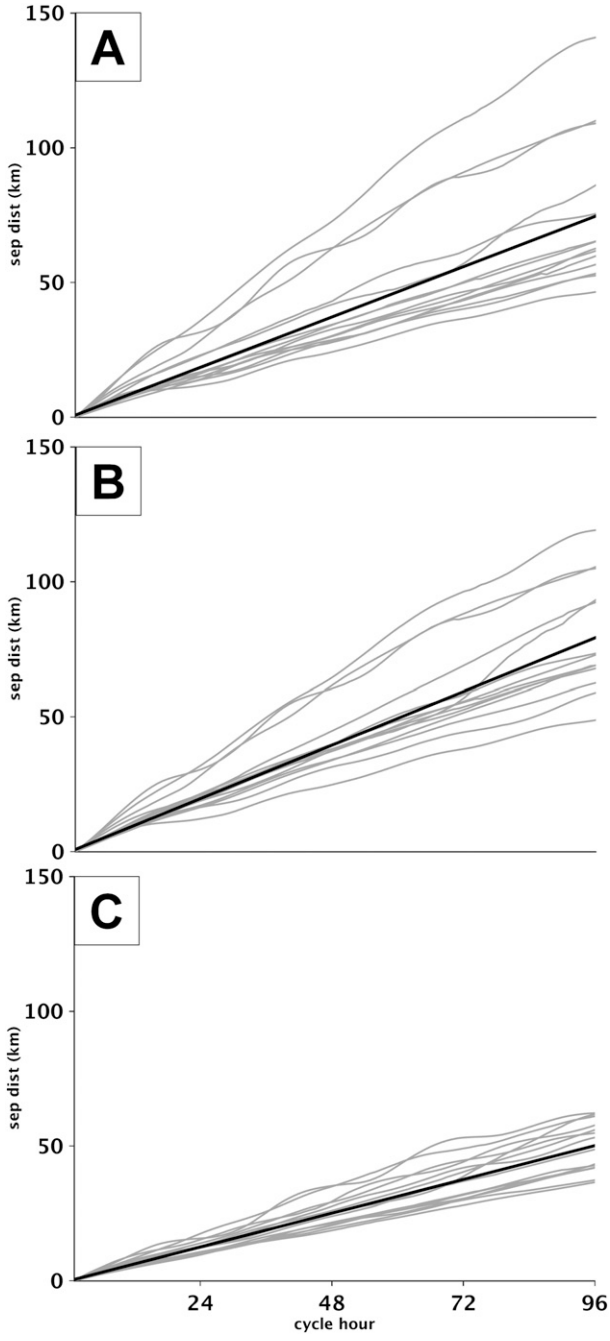

FIG. 6. Mean separation distance as a function of forecast length for each of the 14 assimilation cycles during the two-month study period (gray lines) for the (a) FREE experiment, (b) T/S experiment, and (c) ALL experiment, with the linear fit to all the cycles (black line). The average is taken over all the available drifters for each time step.

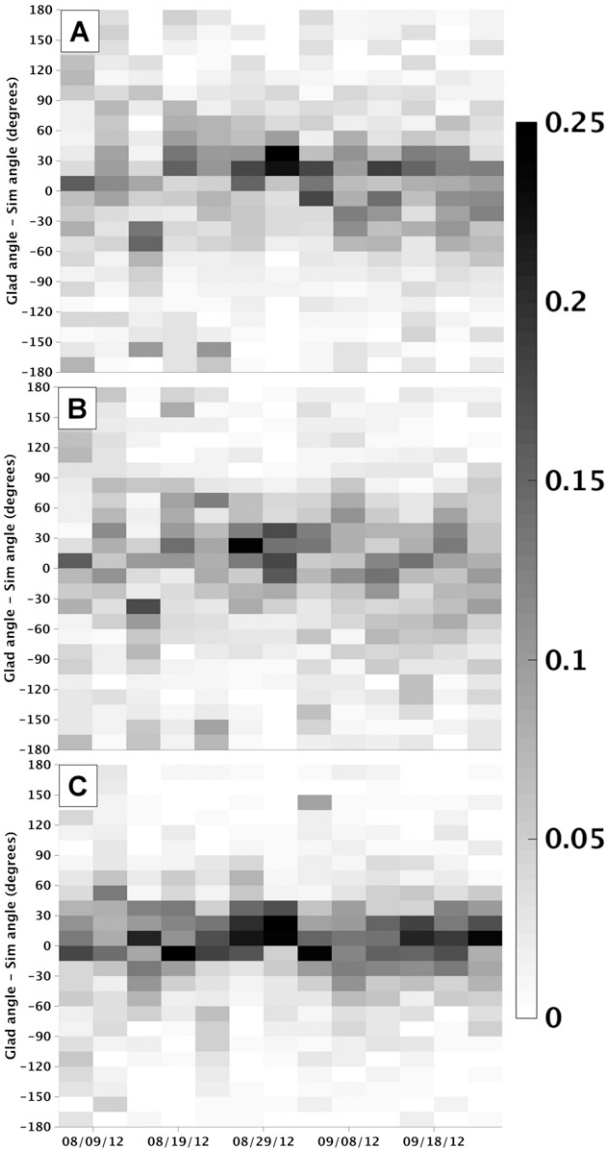

FIG. 7. Two-dimensional histograms showing the percentage of drifters with a given mean angular model-observation mismatch after 24 h for each assimilation cycle. (a) FREE experiment, (b) T/S experiment, and (c) ALL experiment.

calculated only at the locations of the removed drifters and the data-denial experiment is included as well. The data-denial experiment produces significantly lower separation distances than the FREE and T/S runs until the beginning of September. Thereafter the separation distances for the data-denial experiment are of the same order as the FREE and T/S runs, with the ALL experiment producing the lowest distances. As mentioned earlier the removed drifters were in the region of the large eddy whose misplacement causes the large peak in the separation distances of the FREE and T/S runs. Even though the majority of the remaining drifters did not directly sample this eddy, the data-denial experiment still successfully reduces the separation distances because sufficient drifters remained to constrain this eddy feature.

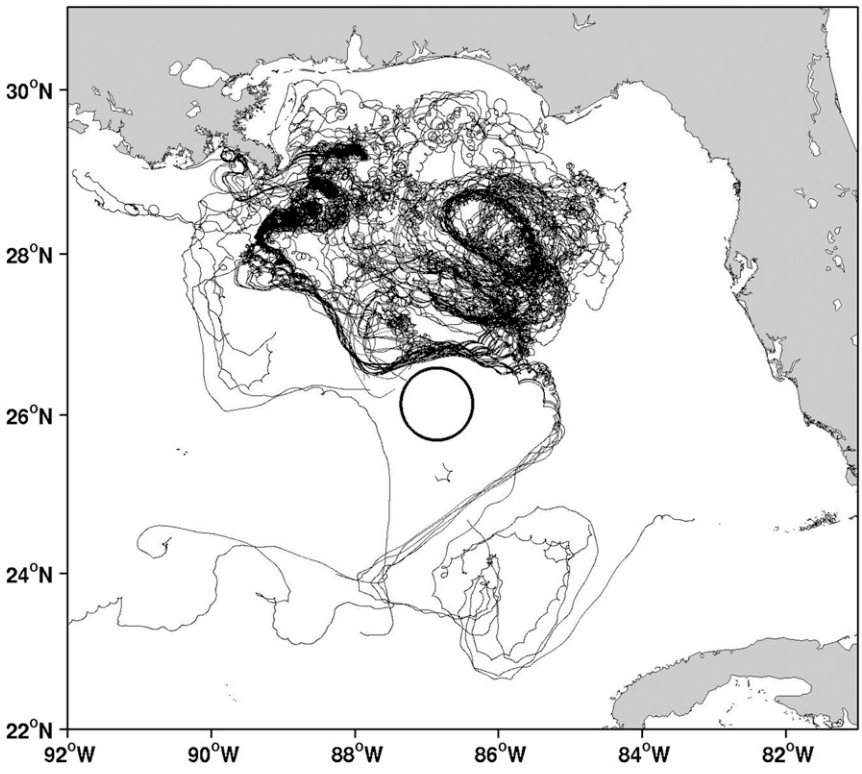

FIG. 8. GLAD drifter trajectories assimilated for the period 1 Aug–30 Sep 2012 for the data-denial experiment. All drifters that ever entered the black circle were removed from the original record.

The improvement of the Lagrangian predictability for the data-denial experiment over the FREE and T/S runs disappears in September (Fig. 9a). This result can be explained by the fact that in this month the distance between unassimilated and assimilated drifters significantly increased. Figure 9b shows the time series of the mean over all unassimilated drifters of the distance to the nearest assimilated drifter for each time step. The large peak near the end of August coincides with the failure of a single assimilated drifter on 27 August, which had been constraining a large number of unassimilated drifters. The hurricane passage around the same time also spread the drifters out spatially. Thus, the period of improved predictability (9–27 August) is marked by an average distance to an assimilated drifter of roughly 15–40 km, whereas during the following period (28 August–29 September) the average distance to an assimilated drifter is much larger, around 60–80 km.

These results suggest that a critical distance above which an assimilated drifter will not sufficiently constrain an unassimilated one is around 40–60 km. It should be cautioned, however, that this critical distance is likely to depend strongly on the flow regime and the dominant scales of circulation features in the area of interest. Moreover, it is likely to be nonisotropic. Clearly, more analysis is needed for a more comprehensive assessment of the spatial scales of a drifter's impact on nearby trajectories, which we hope to report on in follow-on papers.

6. Summary

A previous study (Carrier et al. 2014) showed that assimilating velocity data inferred from drifters using 4DVAR can markedly improve model temperature, salinity, SSH, and velocity Eulerian forecast skill. Here, analysis of the same forecasts described by Carrier et al. (2014) shows that assimilating these drifter velocities also markedly improves trajectory forecast skill over a 24-h period (see Fig. 4). Averages over the fourteen 4-day assimilation cycles studied here show that assimilating drifter velocities reduces trajectory forecast error growth rates by 7.3 km day^{-1}, a substantial improvement (see Fig. 6). Trajectory direction differences also decrease markedly when drifter velocities are assimilated. The data-denial experiment is a first step toward determining the spatial extent of the improvements to Lagrangian predictability. The results show that the

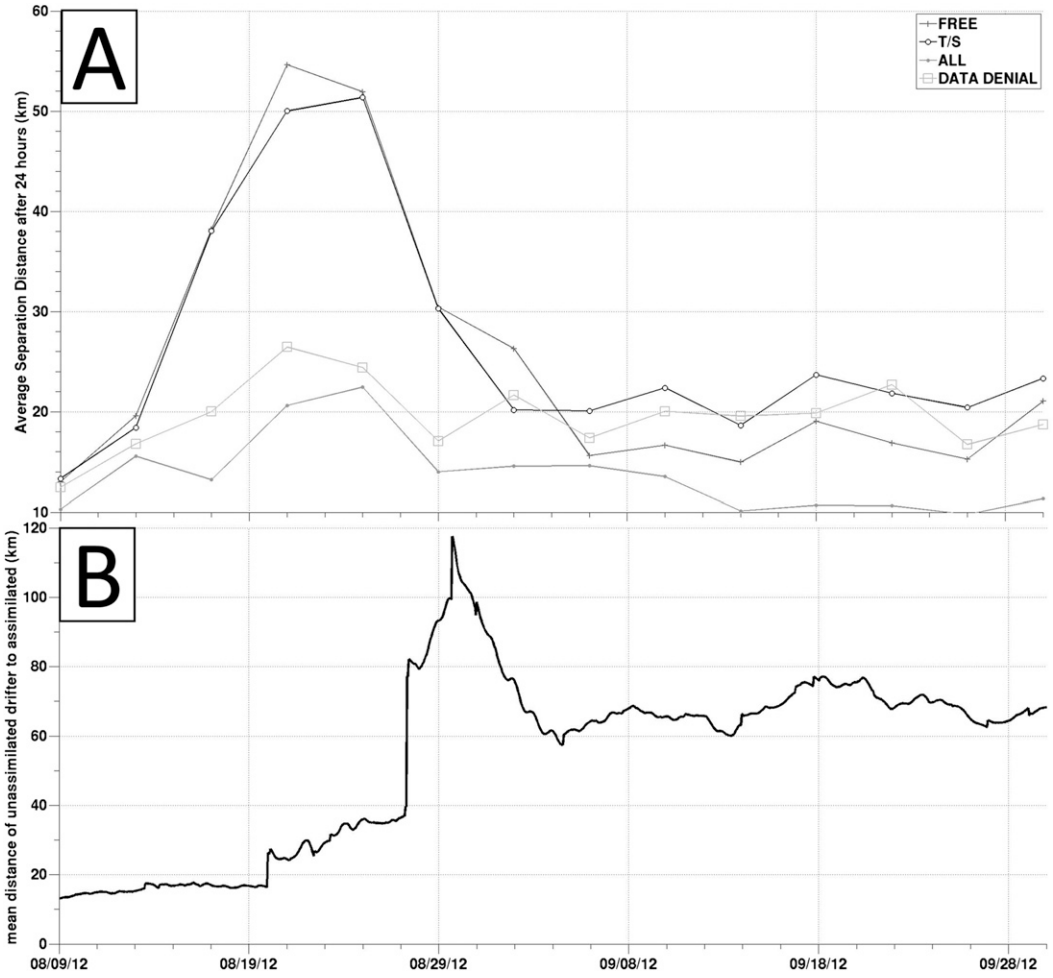

FIG. 9. (a) Mean separation distance (km) after 24 h between the GLAD and simulated drifters for each assimilation cycle. The average is taken only over the drifters removed in the data-denial experiment (cf. Fig. 4). (b) The minimum distance of each unassimilated drifter to the nearest assimilated drifter, averaged over all the unassimilated drifters at each hourly time step.

Lagrangian predictability significantly falls off away from the assimilated drifters for distances greater than about 40 km. Note that the correlation scale selected for these Gulf of Mexico experiments is also 40 km.

Here, the dramatic improvements in mean trajectory forecast skill were due to increased accuracy of the mesoscale forecast position and shape of a large Loop Current ring in the mid-GOM (see Fig. 5). The added constraints provided by assimilated drifter velocities not only improved forecast trajectories, but also provided important corrections to the forecast SSH field.

The tracking and prediction of oil transport at the ocean surface remains a challenging problem for oceanographers. The assimilation of these high-resolution drifter velocities is shown to provide an important correction to the model mesoscale forecast that leads to a substantial improvement in trajectory forecast skill. This result underscores the importance of drifter observations, and their ability to substantially improve model trajectory forecasts in response to future oil spills.

Acknowledgments. This research was made possible in part by a grant from BP/The Gulf of Mexico Research Initiative. B. L. Lipphardt Jr., H. S. Huntley, and A. D. Kirwan Jr. were also supported by the Office of Naval Research MURI OCEAN 3D+1 Grant N00014-11-1-0087. The authors thank CARTHE for providing the GLAD trajectories, and Emanuel Coelho for producing the velocities (derived from these trajectories) used here. Thanks to the CCAR for providing the SSH product in the Gulf of Mexico. We also thank Rich Pawlowicz for providing the freely available M_MAP Matlab toolbox used here.

REFERENCES

Barron, C. N., L. F. Smedstad, J. M. Dastugue, and O. M. Smedstad, 2007: Evaluation of ocean models using observed and simulated drifter trajectories: Impact of sea surface height on synthetic profiles for data assimilation. *J. Geophys. Res.,* **112,** C07019, doi:10.1029/2006JC003982.

Bennett, A. F., 2002: *Inverse Modeling of the Ocean and Atmosphere.* Cambridge University Press, 234 pp.

Carrier, M. J., H. Ngodock, S. Smith, G. Jacobs, P. Muscarella, T. Ozgokmen, B. Haus, and B. L. Lipphardt Jr., 2014: Impact of assimilating ocean velocity observations inferred from Lagrangian drifter data using the NCOM-4DVAR. *Mon. Wea. Rev.,* **142,** 1509–1524, doi:10.1175/MWR-D-13-00236.1.

Chua, B. S., and A. F. Bennett, 2001: An inverse ocean modeling system. *Ocean Modell.,* **3,** 137–165, doi:10.1016/S1463-5003(01)00006-3.

Cummings, J. A., 2005: Operational multivariate ocean data assimilation. *Quart. J. Roy. Meteor. Soc.,* **131,** 3583–3604, doi:10.1256/qj.05.105.

Egbert, G. D., A. F. Bennett, and M. G. G. Foreman, 1994: TOPEX/POSEIDON tides estimated using a global inverse model. *J. Geophys. Res.,* **99,** 24 821–24 852, doi:10.1029/94JC01894.

Huntley, H. S., B. L. Lipphardt Jr., and A. D. Kirwan Jr., 2011: Lagrangian predictability assessed in the East China Sea. *Ocean Modell.,* **36,** 163–178, doi:10.1016/j.ocemod.2010.11.001.

Ide, K., L. Kuznetsov, and C. K. R. T. Jone, 2002: Lagrangian data assimilation for point vortex systems. *J. Turbul.,* **3,** N53, doi:10.1088/1468-5248/3/1/053.

Jacobs, G. A., J. G. Richman, J. D. Doyle, P. L. Spence, B. P. Bartels, C. N. Barron, R. W. Helber, and F. L. Bub, 2014a: Simulating conditional deterministic predictability within ocean frontogenesis. *Ocean Modell.,* **78,** 1–16, doi:10.1016/j.ocemod.2014.02.004.

——, and Coauthors, 2014b: Data assimilation considerations for improved ocean predictability during the Gulf of Mexico Grand Lagrangian Deployment (GLAD). *Ocean Modell.,* **83,** 98–117, doi:10.1016/j.ocemod.2014.09.003.

Kuznetsov, L., K. Ide, and C. K. R. T. Jones, 2003: A method for assimilation of Lagrangian data. *Mon. Wea. Rev.,* **131,** 2247–2260, doi:10.1175/1520-0493(2003)131<2247:AMFAOL>2.0.CO;2.

Martin, P. J., 2000: Description of the Navy Coastal Ocean Model version 1.0. NRL Rep. NRL/FR/7322/00/9962/, 45 pp. [Available from NRL, Code 7322, Bldg. 1009, Stennis Space Center, MS 39529-5004.]

Molcard, A., A. Griffa, and T. M. Özgökmen, 2005: Lagrangian data assimilation in multilayer primitive equation ocean models. *J. Atmos. Oceanic Technol.,* **22,** 70–83, doi:10.1175/JTECH-1686.1.

Ngodock, H. E., 2005: Efficient implementation of covariance multiplication for data assimilation with the representer method. *Ocean Modell.,* **8,** 237–251, doi:10.1016/j.ocemod.2003.12.005.

——, and M. J. Carrier, 2013: A weak constraint 4D-Var assimilation system for the Navy coastal ocean model using the representer method. *Data Assimilation for Atmospheric, Oceanic, and Hydrologic Applications,* Vol. II, S. K. Park and L. Xu, Eds., Springer-Verlag, 367–390, doi:10.1007/978-3-642-35088-7_15.

——, and ——, 2014: A 4DVAR system for the Navy Coastal Ocean Model. Part I: System description and assimilation of synthetic observations in Monterey Bay. *Mon. Wea. Rev.,* **142,** 2085–2107, doi:10.1175/MWR-D-13-00221.1.

Nodet, M., 2006: Variational assimilation of Lagrangian data in oceanography. *Inverse Probl.,* **22,** 245–263, doi:10.1088/0266-5611/22/1/014.

Özgökmen, T. M., A. Molcard, T. M. Chin, L. I. Piterbarg, and A. Griffa, 2003: Assimilation of drifter positions in primitive equation models of midlatitude ocean circulation. *J. Geophys. Res.,* **108,** 3238, doi:10.1029/2002JC001719.

Poje, A. C., and Coauthors, 2014: Submesoscale dispersion in the vicinity of the Deepwater Horizon spill. *Proc. Natl. Acad. Sci. USA,* **111,** 12 693–12 698, doi:10.1073/pnas.1402452111.

Roemmich, D., and Coauthors, 2001: Argo: The global array of profiling floats. *Observing the Oceans in the 21st Century,* C. J. Koblinsky and N. R. Smith, Eds., Melbourne Bureau of Meterorology, 248–258.

Rosmond, T. E., J. Teixeria, M. Peng, T. F. Hogan, and R. Pauley, 2002: Navy Operational Global Atmospheric Prediction Systems (NOGAPS): Forcing for ocean models. *Oceanography,* **15,** 99–108, doi:10.5670/oceanog.2002.40.

Taillandier, V., A. Griffa, P.-M. Poulain, and K. Béranger, 2006: Assimilation of Agro float positions in the north western Mediterranean Sea and impact on ocean circulation simulations. *Geophys. Res. Lett.,* **33,** L11604, doi:10.1029/2005GL025552.

Thompson, K. R., J. Y. Sheng, P. C. Smith, and L. Z. Cong, 2003: Prediction of surface currents and drifter trajectories on the inner Scotian Shelf. *J. Geophys. Res.,* **108,** 3287, doi:10.1029/2001JC001119.

Toner, M., A. D. Kirwan Jr., L. H. Kantha, and J. K. Choi, 2001: Can general circulation models be assessed and their output enhanced with drifter data? *J. Geophys. Res.,* **106,** 19 563–19 579, doi:10.1029/2000JC000587.

Vernieres, G., C. K. R. T. Jones, and I. Kayo, 2011: Capturing eddy shedding in the Gulf of Mexico from Lagrangian observations. *Physica D,* **240,** 166–179, doi:10.1016/j.physd.2010.06.008.

Yu, P., A. L. Kurapov, G. D. Egbert, J. S. Allen, and A. P. Korso, 2012: Variational assimilation of HF radar surface currents in a coastal ocean model off Oregon. *Ocean Modell.,* **49–50,** 86–104, doi:10.1016/j.ocemod.2012.03.001.